

# Antarctic basal environment shaped by high-pressure flow through a subglacial river system

Received: 10 November 2020

C. F. Dow<sup>1,2</sup>✉, N. Ross<sup>3</sup>, H. Jeofry<sup>4,5</sup>, K. Siu<sup>2</sup> and M. J. Siegert<sup>6</sup>

Accepted: 23 September 2022

Published online: 27 October 2022

 Check for updates

The stability of ice sheets and their contributions to sea level are modulated by high-pressure water that lubricates the base of the ice, facilitating rapid flow into the ocean. In Antarctica, subglacial processes are poorly characterized, limiting understanding of ice-sheet flow and its sensitivity to climate forcing. Here, using numerical modelling and geophysical data, we provide evidence of extensive, up to 460 km long, dendritically organized subglacial hydrological systems that stretch from the ice-sheet interior to the grounded margin. We show that these channels transport large fluxes ( $\sim 24 \text{ m}^3 \text{ s}^{-1}$ ) of freshwater at high pressure, potentially facilitating enhanced ice flow above. The water exits the ice sheet at specific locations, appearing to drive ice-shelf melting in these areas critical for ice-sheet stability. Changes in subglacial channel size can affect the water depth and pressure of the surrounding drainage system up to 100 km either side of the primary channel. Our results demonstrate the importance of incorporating catchment-scale basal hydrology in calculations of ice-sheet flow and in assessments of ice-shelf melt at grounding zones. Thus, understanding how marginal regions of Antarctica operate, and may change in the future, requires knowledge of processes acting within, and initiating from, the ice-sheet interior.

The impacts of subglacial hydrology on ice dynamics have been widely demonstrated for Greenland and Alpine glaciers<sup>1,2</sup>. High-pressure water distributed across the ice–bed interface lubricates the ice base, causing enhanced ice flow<sup>2</sup> and, consequently, mass loss and sea-level rise<sup>3</sup>. However, development of large, low-pressure channels during the summer melt season in these environments efficiently removes water, acting to slow ice flow<sup>1</sup>. In contrast to Greenland and Alpine glaciers, the impact of subglacial hydrology on Antarctic ice-sheet dynamics<sup>4–7</sup> remains understudied. The Greenland-style system of seasonally varying hydrological inefficiency/efficiency is driven by surface-water

inputs during the summer (Fig. 1a). By contrast, Antarctic systems are driven entirely by in situ basal water production and so have seasonally stable configurations (Fig. 1b). Antarctic subglacial hydrological systems draining over the grounding line into ice-shelf cavities have been estimated previously through hydraulic potential modelling, assuming time-invariant steady-state water pressures derived solely by ice-overburden pressures<sup>8,9</sup>. Such outlets are often spatially coincident with the location of ice-shelf channels, suggesting that the latter are formed by discharged subglacial water etching upwards into the ice-shelf base<sup>10–12</sup>. Although hydraulic potential modelling allows

<sup>1</sup>Department of Geography and Environmental Management, University of Waterloo, Waterloo, Ontario, Canada. <sup>2</sup>Department of Applied Mathematics, University of Waterloo, Waterloo, Ontario, Canada. <sup>3</sup>School of Geography, Politics and Sociology, Newcastle University, Newcastle upon Tyne, UK.

<sup>4</sup>Faculty of Science and Marine Environment, Universiti Malaysia Terengganu, Kuala Neris, Malaysia. <sup>5</sup>Institute of Oceanography and Environment, Universiti Malaysia Terengganu, Kuala Neris, Malaysia. <sup>6</sup>Grantham Institute and Department of Earth Science and Engineering, Imperial College London, London, UK. ✉e-mail: [christine.dow@uwaterloo.ca](mailto:christine.dow@uwaterloo.ca)

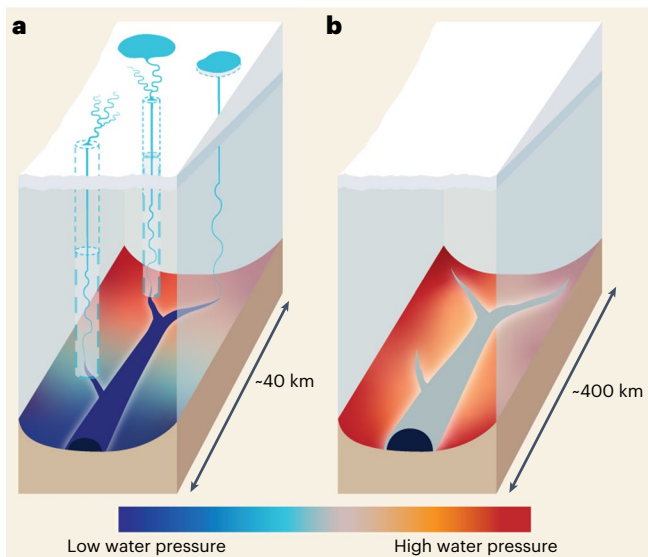


**Fig. 1 | Schematic of subglacial hydrology drainage characteristics for Greenland and Antarctica.** **a**, In Greenland, seasonal surface-water accesses the bed and allows channel development with enough efficiency to lower the water pressure over a distance of tens of kilometres. **b**, In Antarctica, there is no surface-water input, but channels can develop over hundreds of kilometres due to near steady-state inputs. These channels do not lower the surrounding water pressure substantially.

estimates of likely water routing, it does not allow for examination of (1) the presence or size of subglacial channels, (2) how far upstream such channels can persist, (3) the volume and discharge of subglacial water or (4) temporal persistence of the subglacial drainage network. These issues are important for determining the role of subglacial water in modulating Antarctic ice flow and basal melting in ice-shelf ocean cavities, both of which are key for predicting future sea-level rise<sup>13</sup>.

### Antarctic subglacial hydrology modelling

New high-resolution bed topography products from modelled mass conservation techniques<sup>14</sup>, and continent-wide model-derived estimates of basal water production<sup>15</sup>, now enable two-dimensional subglacial hydrology models to be readily applied to large Antarctic catchments. In this Article, we use the finite-element Glacier Drainage System (GlaDS) model<sup>16</sup>, which allows coincident development of inefficient and channelized drainage networks, to assess the basal hydrology of four major ice catchments that feed ice to the Filchner-Ronne Ice Shelf (FRIS) in the Weddell Sea Sector of Antarctica: Institute Ice Stream (IIS); Möller Ice Stream (MIS); Support Force Glacier (SFG); and Foundation Ice Stream/Academy Glacier (FIS-AG) (Methods and Fig. 2). We run GlaDS over these four catchments with a variety of sensitivity tests, including channel and distributed system conductivity, permitting assessment of the extent of channelization and the role that channels play in reducing surrounding water pressure and slowing ice flow (Methods). We present ‘base’ model outputs (Fig. 2b–j and Extended Data Table 1) and compare them with sensitivity test results (Fig. 3 and Extended Data Table 2).

The FIS-AG catchment originates from near South Pole and terminates 750 km downstream at the Filchner–Ronne Ice Shelf. The FIS-AG receives much of its ice through the Pensacola–Pole Basin, which lies up to 2.4 km below sea level (b.s.l.) (with an average elevation of 500 m b.s.l.)<sup>17</sup>. The grounding lines of IIS and MIS are both perched at the top of steep reverse slopes leading into deep basins, more than 1.6 km and 1.7 km b.s.l., respectively<sup>18</sup>. All these regions have been identified as susceptible to marine ice-sheet instability if the grounding zones were to retreat from their current positions<sup>17,18</sup>. SFG is a narrow ice stream

that lies between FIS-AG and Recovery Glacier. It also has a deep basin up to 1.4 km b.s.l. but with a more gentle reverse slope, compared with the other catchments, and a bedrock rise 30 km inland of the grounding zone. Collectively, the IIS, MIS, SFG and FIS-AG is a region of high vulnerability to change<sup>18,19</sup>, has an area of 960,000 km<sup>2</sup> and contains enough ice to raise sea level globally by 4.3 m (ref. 20).

### Extensive network of subglacial channels

Model results indicate that a major subglacial channel exits the grounding line of FIS-AG with a discharge of  $24.2 \text{ m}^3 \text{ s}^{-1}$  and a cross-sectional area (CSA) of 11.7 m<sup>2</sup> (Fig. 2c). This channel comprises two major branches: the primary branch is from AG and has a total length of 460 km; the secondary branch drains FIS and flows for 130 km before merging with the Academy channel (Fig. 2c,f). Major channels also exit at IIS (discharge:  $8.3 \text{ m}^3 \text{ s}^{-1}$ ; CSA: 5.0 m<sup>2</sup>; Fig. 2d) and MIS (discharge:  $3.9 \text{ m}^3 \text{ s}^{-1}$ ; CSA: 2.7 m<sup>2</sup>; Fig. 2d), with SFG draining two smaller channels (discharge: 0.51 and  $0.45 \text{ m}^3 \text{ s}^{-1}$ ; CSA: 0.45 and 0.37 m<sup>2</sup>; Fig. 2b). All these channels are persistent annually. The size and distribution of channels draining water beneath the four ice streams/glacier catchments remain resistant to changes in sensitivity tests; the only major variation observed is a shift in the initiation of the extensive AG channel by  $\pm 15 \text{ km}$  (Fig. 3b,d). The lengths of these channels dwarf those of the nearby Recovery Glacier, where hydrological modelling suggests channels up to 75 km long between connected subglacial lakes<sup>4</sup>. The FIS-AG channels also connect several lakes<sup>21</sup> but persist downstream of these features to drain into the FRIS ocean cavity (Fig. 2f).

FIS-AG subglacial channels have previously been inferred from radar data<sup>22</sup> with high reflectivity indicating the presence of water. We find good correspondence between the locations of high reflectivity and the modelled subglacial channels (Extended Data Fig. 1). Radar surveys near the grounding line of SFG also record the presence of a subglacial channel that was identifiable up to 7.7 km upstream of the grounding line, after which it could no longer be differentiated from the surrounding basal conditions<sup>23</sup>. The location and length of this channel correspond with the more easterly modelled channel at SFG (Fig. 2b,e), which runs from 5 km upstream of the grounding zone.

These basal drainage networks resemble dendritic channelized subglacial systems identified in summer Alpine and Greenlandic environments<sup>24,25</sup>, despite the absence of surface-water inputs. However, the FIS-AG, SFG, MIS and IIS channels (Fig. 2c) extend much farther inland than those monitored<sup>1</sup> and modelled<sup>26</sup> in Greenland at ~40 km (Fig. 1a), and they persist year-round.

### High-pressure Antarctic channels

Subglacial channels typically develop at a lower pressure than the surrounding distributed drainage system due to faster melt rates from viscous water flow compared with ice overburden-driven creep closure<sup>1,24</sup>. However, although our modelled Antarctic subglacial channels have lower water pressure than the adjacent distributed system, they operate close to overburden pressure (at around 98%), near steady state (Fig. 2h–j). We test the impact of this on the distributed drainage system and related ice-dynamic drivers by comparing the channel flux, water pressure and water depth in sensitivity tests with higher and lower channel conductivities. Lower conductivity ( $0.01 \text{ m}^{3/2} \text{ kg}^{-1/2}$ ) inhibits channel formation and lowers the discharge from the FIS-AG grounding-line subglacial channel discharge by  $\sim 12 \text{ m}^3 \text{ s}^{-1}$  (Extended Data Table 2). These channels remain at a similar pressure to those in the higher-conductivity systems. However, the impact of smaller and less-efficient channels on the hydrological system extends far beyond the channelized drainage routes, up to 100 km on either side of the primary channels (Fig. 3b,c). The distributed water system in these areas sees an increase in pressure, but generally by less than 5% of overburden (which in this region translates to  $\sim 0.4 \text{ MPa}$ ). In addition, water depth in the distributed system increases up to 3 cm, other than in deep basins where subglacial lakes occur and where water depth increases

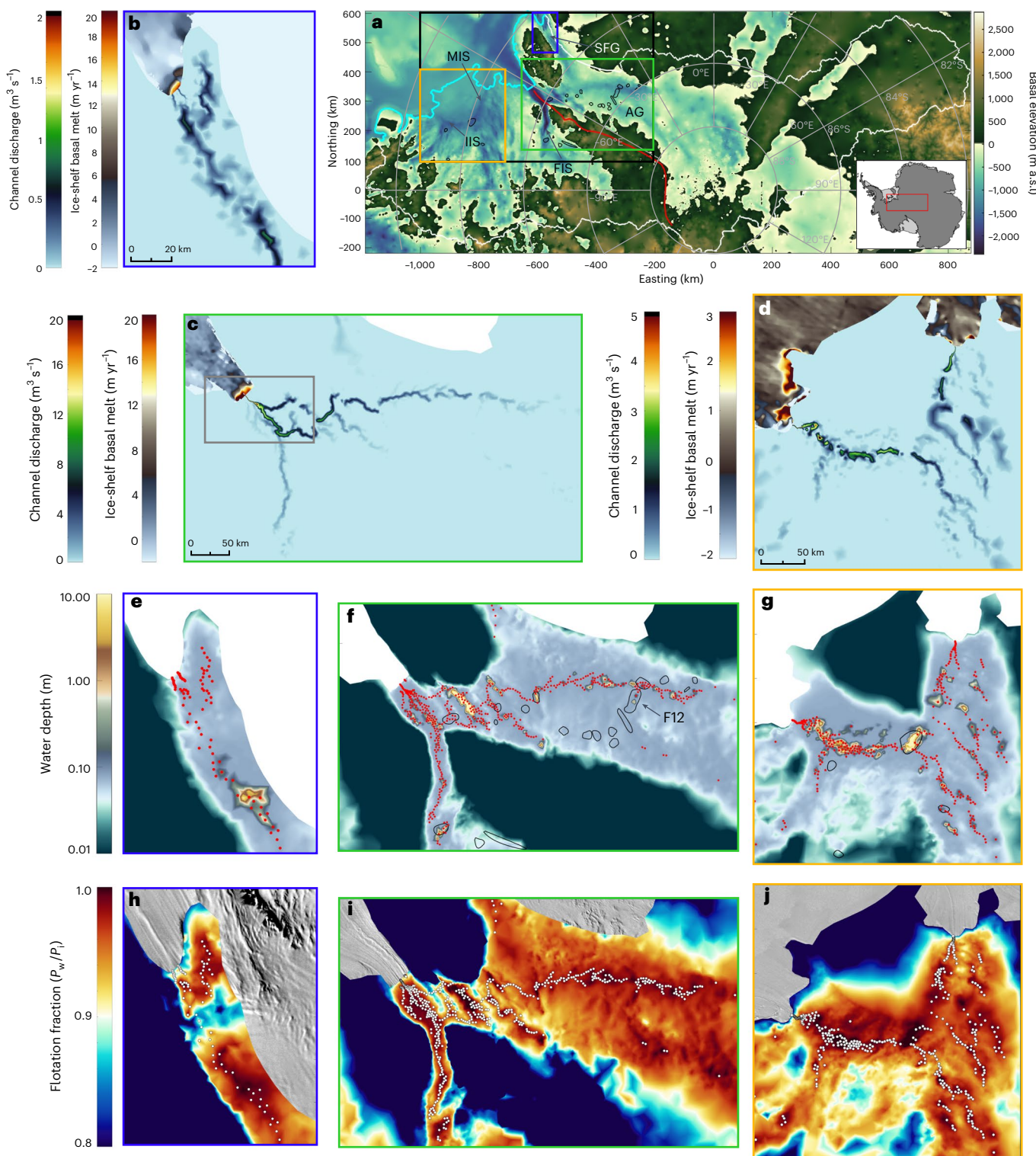


**Fig. 2 | Modelled subglacial hydrology.** **a**, Basal topography<sup>14</sup> of the study region with the model domain outlined in white and the grounding line<sup>42</sup> in cyan (plotted as m above sea level (a.s.l.)). The divide between West and East Antarctic Ice Sheets is plotted in red, and the locations of ICESat lakes<sup>21</sup> are outlined in black. The black box shows the extent of Fig. 3. **b–d**, Ice-shelf melt rates from Cryosat-2 altimetry measurements<sup>36</sup> and modelled channel discharge for **(b)** SFG, **(c)** FIS-AG and **(d)** IIS and MIS. The grey box in **c** shows the extent of Extended Data Fig. 1.

**e–g**, Distributed system water depth (with a log scale) with channels plotted in red and the locations of ICESat lakes<sup>21</sup> outlined in black for **(e)** SFG, **(f)** FIS-AG and **(g)** IIS and MIS. **h–j**, Water pressure ( $P_w$ ) plotted as a fraction of overburden ( $P_i$ ) for **(h)** SFG, **(i)** FIS-AG and **(j)** IIS and MIS. White circles are locations of channels with discharge  $>0.2 \text{ m}^3 \text{s}^{-1}$ . Background image is the ice-surface moderate-resolution imaging spectroradiometer mosaic<sup>43</sup>. Regions identified by colour rectangles in **a** are identified by their respective outlines in **b–j**.

by up to several metres as a result of fewer or smaller channels forming (Fig. 3c). For example, lake F12 (Fig. 2f) has a maximum water depth of ~4 m in the ‘base’ model run, but this increases to 16 m in the low

channel conductivity run. Given that satellite-derived altimetry data suggest F12 changes in depth by ~6 m over a drainage cycle<sup>27</sup>, the base model outputs are probably more applicable than the low conductivity

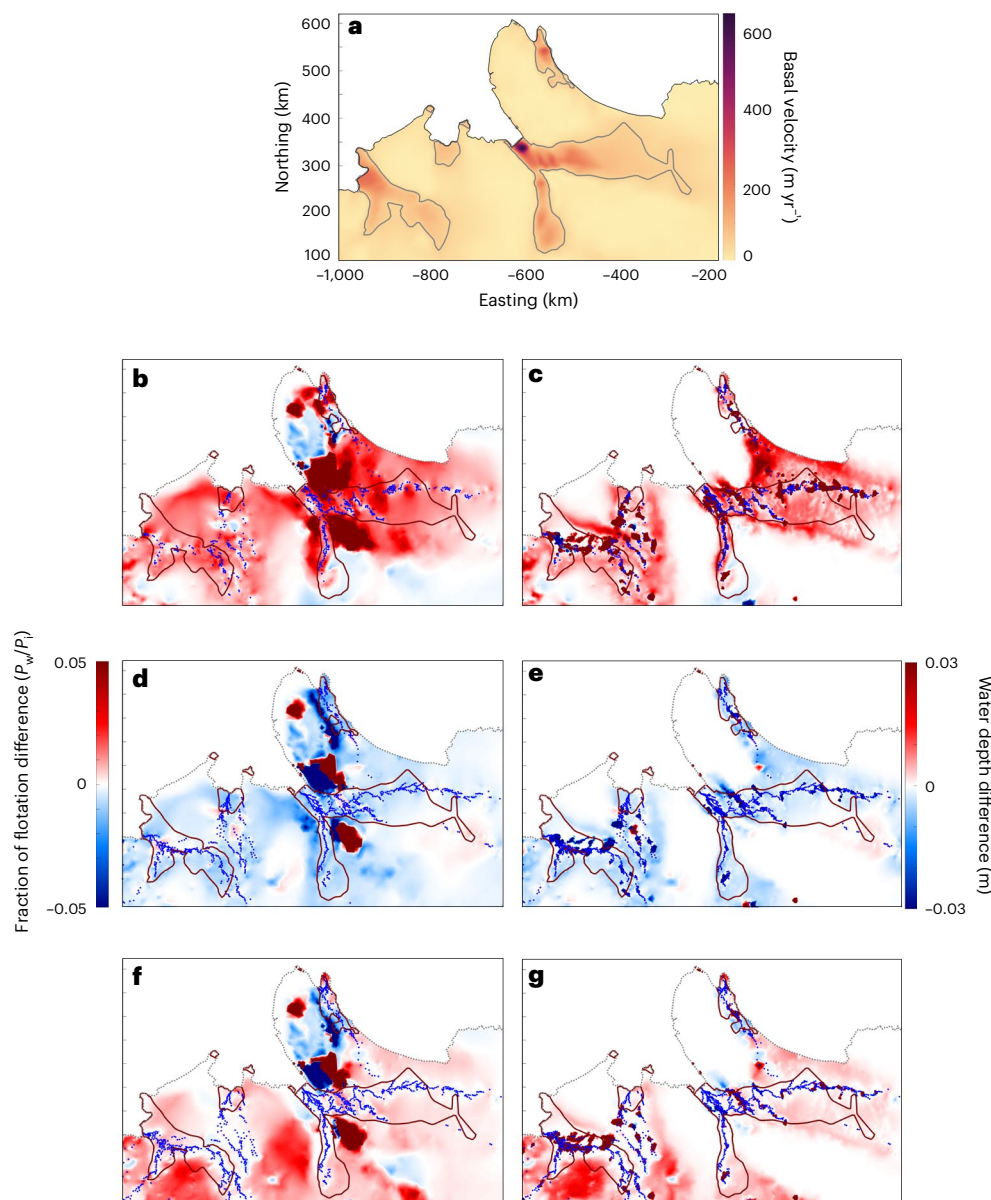


**Fig. 3 | Impact of channel efficiency on system pressure and water depth.**

**a**, Basal velocity from Ice-Sheet and Sea-Level System Model (ISSM)<sup>15</sup> with the 50 m  $\text{yr}^{-1}$  contour outlines in grey. **b,c**, Difference between a system with lower channel conductivity and the standard (base) model run for (**b**) fraction of flotation and (**c**) water depth. **d,e**, Difference between a system with higher channel conductivity and the standard model run for (**d**) fraction of flotation and

(**e**) water depth. **f,g**, Difference between a system with additional (1.5 times) basal water and the standard model run for (**f**) fraction of flotation and (**g**) water depth. The 50 m  $\text{yr}^{-1}$  basal velocity contour is outlined in dark red on each plot. The blue dots are the channels for the low conductivity (**b,c**), higher conductivity (**d,e**) and additional basal water (**f,g**) runs. These plots include information for IIS, MIS, FIS-AG and SFG, with the extent shown by the black box in Fig. 2a.

outputs. Higher channel conductivity ( $0.1 \text{ m}^{3/2} \text{ kg}^{-1/2}$ ) compared with the base run impacts water depth and pressure over a similarly wide region, although only decreasing distributed water depth  $<0.5 \text{ cm}$  (Fig. 3e) and pressure  $<1\%$  of overburden (Fig. 3d), on average.

High-pressure Antarctic channels are fundamentally different from those in Greenland and play a distinct role in Antarctic glaciology. In Greenland, channels that grow and shrink annually adjust regularly to changing hydrological conditions<sup>28</sup> and operate at pressures substantially lower than the surrounding distributed system (dropping to  $\sim 40\%$  of overburden<sup>1</sup>; Fig. 1a). The low-pressure Greenland channels thus play a key role in limiting ice-flow rates by drawing water from adjacent high-pressure regions, reducing the amount of basal lubrication<sup>1</sup>. In Antarctica, however, subglacial channels have limited dynamical influence on short temporal scales but are maintained at near steady-state with a high-pressure distributed water system

adjacent to the channels (Fig. 1b). Changes in channel size currently occur only in response to subglacial lake growth and drainage over periods of years<sup>21</sup>. These channels are, however, critical for transferring water from the ice-sheet interior to the grounding zone, and any alteration in channel efficiency, size or pressure can impact large swathes of the basal Antarctic system and, consequently, ice-flow rates and processes operating at grounding zones.

### High-pressure water drives fast ice flow

FIS-AG has both the largest hydrological catchment and the fastest surface ice flow ( $500\text{--}600 \text{ m yr}^{-1}$ ) within the model domain. IIS has the next largest catchment and next fastest flow ( $350 \text{ m yr}^{-1}$ ), followed by SFG ( $290 \text{ m yr}^{-1}$ ) and then MIS ( $130 \text{ m yr}^{-1}$ ). All these enhanced ( $>25 \text{ m yr}^{-1}$ ) flow regions correspond with modelled water pressures of 96% of overburden or above (Figs. 2h–j and 3a). In glacial settings, regions of faster

ice flow are often assumed to be driven by high-pressure distributed basal water systems with a lack of large, efficient channels<sup>1,2</sup> and/or by steep surface slopes creating large driving stresses<sup>29</sup>. In the Antarctic, the fastest flowing regions are ice streams that drain large volumes of ice into the ocean<sup>30</sup> and have shallow surface gradients and therefore limited driving stress<sup>29</sup>. The latter suggests that high-pressure distributed drainage plays a key role in Antarctic fast flow, yet variability in ice-shelf topography at the grounding line, along with our modeling, provides strong evidence of large focused channels exiting many ice streams<sup>10,11</sup>. Our model results explain how this is possible, with high-pressure subglacial water coincident with regions of fast ice flow and the presence of channels.

In a warming climate, thinning at the grounding zone could increase the driving stress upstream due to steeper ice-surface gradients, facilitating faster flow<sup>31</sup> and an increase in frictional basal water production. In addition, warming air temperatures could, potentially, allow seasonal access of water from the ice surface to the ice bed<sup>32,33</sup>. We test the impact of increased basal water volumes by multiplying the basal water production rate by 150%. We find that water pressure, and therefore potentially ice-flow speed, increases in the interior regions of the catchment (Fig. 3f). Immediately adjacent to the channels (10–40 km to either side), increasing the water supply has limited impact on water pressure and therefore, by inference, sliding velocity (Fig. 3f). However, in regions where fast flow is observed, pressures beyond this region increase by 1–3% of overburden. This suggests that increased basal water availability may not greatly change the dynamics of the ice near the location of channels under the current ice configuration. However, ice flowing over the more distant distributed system may accelerate. Conversely, simultaneous changes in ice-surface slope and/or greater volumes of water input on a seasonal basis could enhance efficient channel formation. This would draw more water from the pressurized distributed system, particularly when variations in surface-water input prevent channels from reaching steady state.

## Large water volume into ice-shelf cavity

The volume of water discharged into the FRIS ice-shelf cavity varies between outlets. At the FIS-AG grounding line, the subglacial channel discharges a constant  $24.2 \text{ m}^3 \text{ s}^{-1}$  of freshwater. This is considerably larger than the calculated discharge from smaller subglacial channels draining IIS ( $8.3 \text{ m}^3 \text{ s}^{-1}$ ), MIS ( $3.9 \text{ m}^3 \text{ s}^{-1}$ ) and SFG ( $0.51$  and  $0.45 \text{ m}^3 \text{ s}^{-1}$ ). These differential discharge rates are due to catchment size and basal melt rates (Extended Data Fig. 2 and Extended Data Table 3). Given that the catchment size of MIS is 1/20 that of FIS-AG, it is initially surprising that its grounding-line hydraulic discharge is -1/6 of FIS-AG. However, this is due to the location of the MIS catchment in a region of relatively high water production ( $4.8 \text{ m}^3 \text{ s}^{-1}$ ). All the ice streams lose a portion of their basal water through freezing, and some of the supply is discharged over the grounding line by the distributed system rather than the primary drainage channels. However, the FIS-AG has greater volumes of water ( $-4.9 \text{ m}^3 \text{ s}^{-1}$ ) discharging from the grounding zone than produced from geothermal and ice-bed frictional heating alone. This is due to melting within the 460-km-long channel.

The grounding-zone outlet locations for the subglacial channels of FIS-AG (Fig. 2i), IIS and MIS (Fig. 2j) and SFG (Fig. 2h) each coincide with major ice-shelf basal channels (Methods and Extended Data Figs. 3 and 4). In general, higher discharge over the grounding line appears to lead to larger sub-ice-shelf channels (Fig. 2b–d, Extended Data Figs. 3 and 4 and Extended Data Table 3). The importance of subglacial discharge for ice-shelf melting can also be evaluated by comparing melt rates calculated from ocean models with those inferred by satellite altimetry. Ocean modelling suggests FIS-AG and SFG grounding zones have higher melt rates than IIS and MIS due to their deeper grounding lines, which decrease the pressure melt temperature and allow access of high-salinity shelf water to the base of the ice<sup>34,35</sup>. However, at the channel outlets, the ocean modelling consistently predicts lower

melt rates compared with the estimates from Cryosat-2-derived melt mapping<sup>36</sup> (Fig. 2b–d and Extended Data Table 3). At FIS-AG and SFG, there is an order of magnitude difference between modelled ice-shelf melt rates ( $2.9 \text{ m yr}^{-1}$  and  $2.8 \text{ m yr}^{-1}$  (ref. <sup>37</sup>) and satellite-derived rates ( $26.43 \text{ m yr}^{-1}$  and  $18.5 \text{ m yr}^{-1}$ , respectively<sup>36</sup>; Fig. 2b,c). By contrast, 10 km downstream of the grounding zone of SFG, within an ice-shelf channel, there is consistency among ocean modelling<sup>37</sup>, Cryosat-2 altimetry<sup>36</sup> and measured<sup>38</sup> melt rates of  $-1.6 \text{ m yr}^{-1}$ . The high Cryosat-2 melt rates at the grounding-zone channel outlets<sup>36</sup> demonstrate that subglacial discharge into ice-shelf cavities should be included in ocean models directed towards assessing ice-shelf melt.

Ocean models run until the year 2199 show enhanced melt, particularly at the deep grounding lines of FIS-AG and SFG<sup>35</sup>. This modelling did not consider subglacial outflow, however, which would enhance melt at the base of the ice shelf, with the fresh, buoyant water exiting over the grounding line drawing Modified Warm Deep Water to the ice-shelf base. This would increase ice-shelf melt rates at the channel outlets beyond rates currently calculated or predicted over the next 200 years<sup>36,39</sup>. The effects of enhanced ice-shelf melt could cause (1) grounding-line retreat beyond that predicted by ocean modelling<sup>35</sup>; (2) larger ice-shelf channels, as demonstrated by the relationship between current subglacial discharge and ice-shelf profiles, which could weaken the ice shelf and cause fracturing<sup>40</sup>; and (3) a reduction in ice-shelf buttressing, causing acceleration and thinning of the upstream grounded ice<sup>31</sup>. The latter would drive enhanced frictional melt at the grounded ice base and direct greater volumes of water into subglacial channels in response to steeper surface-driven hydraulic potential gradients. Additional water flux over the grounding line could then instigate a positive feedback effect, enhancing all of the preceding processes.

## Impact of Antarctic subglacial channels

Antarctic subglacial hydrological channels play a key role in efficiently funnelling water from the interior of subglacial catchments towards the grounding line, despite maintaining high pressures at all times. The persistent near steady-state nature of current Antarctic channels allows them to operate at water pressures much closer to overburden than their equivalent in Alpine or Greenland settings. The accumulation of high-pressure water drives fast ice flow in the grounded areas, with the channels concentrating a flux of freshwater into ice-shelf ocean cavities, facilitating enhanced melt of ice shelves by buoyantly drawing up warm, deep water. Currently, basal water supply is controlled over large catchments by a combination of geothermal heat flux and friction related to the basal flow of ice. The former will change only over geological timescales, but the latter is liable to alter notably over the next century if ice-shelf buttressing is reduced and upstream grounded ice speeds up. Such acceleration will change both the ice-surface slope and basal water production. Furthermore, as Antarctic air temperatures warm over the next century, additional water will potentially reach the ice-bed interface from the surface. Changes to basal water supply will impact the capacity of basal channels, which we demonstrate affects the distributed system pressure up to 100 km on either side of primary channel routes, and, in the case of seasonal inputs, could move the Antarctic system away from steady state towards a Greenland-like system. Consequently, predictions by ice-sheet and ocean models of ice-sheet evolution as a result of climate warming, especially under strong global warming scenarios, must account for the influence of hydrology on ice dynamics in ways not presently adopted<sup>41</sup>.

## Online content

Any methods, additional references, Nature Research reporting summaries, source data, extended data, supplementary information, acknowledgements, peer review information; details of author contributions and competing interests; and statements of data and code availability are available at <https://doi.org/10.1038/s41561-022-01059-1>.

## References

1. Nienow, P., Sole, A., Slater, D. A. & Cowton, T. Recent advances in our understanding of the role of meltwater in the Greenland Ice Sheet system. *Curr. Clim. Change Rep.* **3**, 330–344 (2017).
2. Iken, A. & Bindschadler, R. A. Combined measurements of subglacial water pressure and surface velocity of Findelengletscher, Switzerland: conclusions about drainage system and sliding mechanism. *J. Glaciol.* **32**, 101–119 (1986).
3. Flowers, G. E. Hydrology and the future of the Greenland Ice Sheet. *Nat. Commun.* **9**, 2729 (2018).
4. Dow, C. F. et al. Dynamics of active subglacial lakes in Recovery Ice Stream. *J. Geophys Res. Earth.* **123**, 837–850 (2018).
5. Dow, C. F. et al. Totten Glacier subglacial hydrology determined from geophysics and modeling. *Earth Planet Sci. Lett.* **531**, 115961 (2020).
6. Stearns, L. A., Smith, B. E. & Hamilton, G. S. Increased flow speed on a large East Antarctic outlet glacier caused by subglacial floods. *Nat. Geosci.* **1**, 827–831 (2008).
7. Siegfried, M. R., Fricker, H. A., Carter, S. P. & Tulaczyk, S. Episodic ice velocity fluctuations triggered by a subglacial flood in West Antarctica. *Geophys. Res. Lett.* **43**, 2640–2648 (2016).
8. Livingstone, S., Clark, C., Woodward, J. & Kingslake, J. Potential subglacial lake locations and meltwater drainage pathways beneath the Antarctic and Greenland Ice Sheets. *Cryosphere* **7**, 1721–1740 (2013).
9. Willis, I. C., Pope, E. L., Gwendolyn, J. M., Arnold, N. S. & Long, S. Drainage networks, lakes and water fluxes beneath the Antarctic ice sheet. *Ann. Glaciol.* **57**, 96–108 (2016).
10. Le Brocq, A. M. et al. Evidence from ice shelves for channelized meltwater flow beneath the Antarctic Ice Sheet. *Nat. Geosci.* **6**, 945–948 (2013).
11. Alley, K. E., Scambos, T. A., Siegfried, M. R. & Fricker, H. A. Impacts of warm water on Antarctic ice shelf stability through basal channel formation. *Nat. Geosci.* **9**, 290–293 (2016).
12. Marsh, O. J. et al. High basal melting forming a channel at the grounding line of Ross Ice Shelf, Antarctica. *Geophys. Res. Lett.* **43**, 250–255 (2016).
13. Siegert, M. J., Alley, R. B., Rignot, E., Englander, J. & Corell, R. 21st century sea-level rise could exceed IPCC predictions for strong-warming futures. *One Earth* **3**, 691–703 (2020).
14. Morlighem, M. et al. Deep glacial troughs and stabilizing ridges unveiled beneath the margins of the Antarctic Ice Sheet. *Nat. Geosci.* **13**, 132–137 (2020).
15. Seroussi, H. et al. initMIP-Antarctica: an ice sheet model initialization experiment of ISMIP6. *Cryosphere* **13**, 1441–1471 (2019).
16. Werder, M. A., Hewitt, I. J., Schoof, C. G. & Flowers, G. E. Modeling channelized and distributed subglacial drainage in two dimensions. *J. Geophys Res. Earth.* **118**, 2140–2158 (2013).
17. Paxman, G. J. et al. Subglacial geology and geomorphology of the Pensacola-Pole basin, East Antarctica. *Geochem Geophys Geosyst.* **20**, 2786–2807 (2019).
18. Ross, N. et al. Steep reverse bed slope at the grounding line of the Weddell Sea sector in West Antarctica. *Nat. Geosci.* **5**, 393–396 (2012).
19. Wright, A. P. et al. Sensitivity of the Weddell Sea sector ice streams to sub-shelf melting and surface accumulation. *Cryosphere* **8**, 2119–2134 (2014).
20. Rignot, E. et al. Four decades of Antarctic Ice Sheet mass balance from 1979–2017. *Proc. Natl Acad. Sci. USA* **116**, 1095–1103 (2019).
21. Smith, B. E., Fricker, H. A., Joughin, I. R. & Tulaczyk, S. An inventory of active subglacial lakes in Antarctica detected by ICESat (2003–2008). *J. Glaciol.* **55**, 573–595 (2009).
22. Jeofry, H. et al. Hard rock landforms generate 130 km ice shelf channels through water focusing in basal corrugations. *Nat. Commun.* **9**, 4576 (2018).
23. Hofstede, C. et al. Evidence for a grounding line fan at the onset of a basal channel under the ice shelf of Support Force Glacier, Antarctica, revealed by reflection seismics. *Cryosphere* **15**, 1517–1535 (2021).
24. Fountain, A. G. & Walder, J. S. Water flow through temperate glaciers. *Rev. Geophys.* **36**, 299–328 (1998).
25. Chu, V. W. Greenland Ice Sheet hydrology: a review. *Prog. Phys. Geogr.* **38**, 19–54 (2014).
26. Cook, S. J., Christoffersen, P., Todd, J., Slater, D. & Chauché, N. Coupled modelling of subglacial hydrology and calving-front melting at Store Glacier, West Greenland. *Cryosphere* **14**, 905–924 (2020).
27. Siegfried, M. R. & Fricker, H. A. Illuminating active subglacial lake processes with ICESat-2 laser altimetry. *Geophys. Res. Lett.* **48**, e2020GL091089 (2021).
28. Schoof, C. Ice-sheet acceleration driven by melt supply variability. *Nature* **468**, 803–806 (2010).
29. Truffer, M. & Echelmeyer, K. A. Of isbrae and ice streams. *Ann. Glaciol.* **36**, 66–72 (2003).
30. Rignot, E., Mouginot, J. & Scheuchl, B. Ice flow of the Antarctic Ice Sheet. *Science* **333**, 1427–1430 (2011).
31. Seroussi, H. et al. ISMIP6 Antarctica: a multi-model ensemble of the Antarctic Ice Sheet evolution over the 21st century. *Cryosphere* **14**, 3033–3070 (2020).
32. Trusel, L. D. et al. Divergent trajectories of Antarctic surface melt under two twenty-first-century climate scenarios. *Nat. Geosci.* **8**, 927–932 (2015).
33. Nowicki, S. et al. Experimental protocol for sea level projections from ISMIP6 stand-alone ice sheet models. *Cryosphere* **7**, 2331–2368 (2020).
34. Nicholls, K. W., Østerhus, S., Makinson, K., Gammelsrød, T. & Fahrbach, E. Ice–ocean processes over the continental shelf of the southern Weddell Sea, Antarctica: a review. *Rev. Geophys.* **47**, RG3003 (2009).
35. Timmermann, R. & Goeller, S. Response to Filchner–Ronne Ice Shelf cavity warming in a coupled ocean–ice sheet model—Part 1: the ocean perspective. *Ocean Sci.* **13**, 765–776 (2017).
36. Adusumilli, S., Fricker, H. A., Medley, B., Padman, L. & Siegfried, M. R. Interannual variations in meltwater input to the Southern Ocean from Antarctic ice shelves. *Nat. Geosci.* **13**, 616–620 (2020).
37. Mueller, R. D., Hattermann, T., Howard, S. L. & Padman, L. Tidal influences on a future evolution of the Filchner–Ronne Ice Shelf cavity in the Weddell Sea, Antarctica. *Cryosphere* **12**, 453–476 (2018).
38. Humbert, A. et al. On the evolution of an ice shelf melt channel at the base of Filchner Ice Shelf, from observations and viscoelastic modeling. *Cryosphere* **16**, 4107–4139 (2022).
39. Jenkins, A. Convection-driven melting near the grounding lines of ice shelves and tidewater glaciers. *J. Phys. Oceanogr.* **41**, 2279–2294 (2011).
40. Dow, C. F. et al. Basal channels drive active surface hydrology and transverse ice shelf fracture. *Sci. Adv.* **4**, eaao7212 (2018).
41. Pattyn, F. & Morlighem, M. The uncertain future of the Antarctic Ice Sheet. *Science* **367**, 1331–1335 (2020).
42. Bindschadler, R. et al. Getting around Antarctica: new high-resolution mappings of the grounded and freely-floating boundaries of the Antarctic Ice Sheet created for the International Polar Year. *Cryosphere* **5**, 569–588 (2011).
43. Haran, T., Bohlander, J., Scambos, T., Painter, T. & Fahnestock, M. MODIS Mosaic of Antarctica 2008–2009 (MOA2009) Image Map Version 1 (National Snow and Ice Data Center, 2014).

**Publisher's note** Springer Nature remains neutral with regard to jurisdictional claims in published maps and institutional affiliations.

Springer Nature or its licensor holds exclusive rights to this article under a publishing agreement with the author(s) or other

rightholder(s); author self-archiving of the accepted manuscript version of this article is solely governed by the terms of such publishing agreement and applicable law.

© The Author(s), under exclusive licence to Springer Nature Limited 2022

## Methods

### Subglacial hydrology modelling

GlaDS has previously been applied to hydrological catchments elsewhere in the Antarctic, including Recovery Glacier<sup>4</sup>, the Aurora Subglacial Basin and Totten Glacier<sup>5</sup>, David Glacier<sup>44</sup> and Getz Ice Shelf hydrological catchment<sup>45</sup>. The model set-up and equations are described in depth in ref. <sup>16</sup>; model parameters used here are listed in Extended Data Table 1.

GlaDS is a finite-element model and includes distributed system development across triangular elements, which exchange water with element edges where basal channels can develop. The model therefore has dynamic drainage evolution both spatially and temporally. There is some network dependency on mesh sizing, but it has been shown to have negligible impacts on the outcomes of catchment-scale hydrological assessments, although there may be some local impacts on individual subglacial lake drainage dynamics<sup>46</sup>.

GlaDS is initialized with no basal channels, and these form over time due to water flux from the surrounding distributed drainage elements. In a situation with slow flow over the elements, which could be caused by minimal gradients in hydraulic potential and/or limited water supply, channels will form less readily. The equation for channel development is:

$$\frac{\partial S}{\partial t} = \frac{|Q| - (c_t c_w P_w Q)}{\rho_i L} - A_c S |N|^{n-1} N$$

where  $Q$  is the channel discharge,  $\epsilon$  is the hydraulic potential over distance  $s$ ,  $c_t$  is the Clapeyron slope,  $c_w$  is the specific heat capacity of water,  $P_w$  is the density of water,  $P_w$  is water pressure, which is determined from the pressure in the adjacent distributed system elements,  $\rho_i$  is the density of ice,  $L$  is the latent heat of fusion,  $A_c$  is the ice rheological constant,  $N$  is the effective pressure and  $n$  is Glen's flow constant. Channels open through viscous dissipation of heat generated by the speed of water flow, itself driven by a combination of the hydraulic potential gradient and the channel conductivity; the latter is an unknown frictional parameter and therefore one that we explore with sensitivity testing. Channels close through ice creep. As channels can form on all element edges, we define the threshold when we call an element edge flow feature a 'channel' as having a discharge of  $>0.2 \text{ m}^3 \text{ s}^{-1}$ .

In our model experiments, we include freezing and melting within both the distributed and channelized systems<sup>47</sup>. Water production rates are sufficiently low that basal freeze-on could be an important factor in how the subglacial hydrological system develops; for example, we found that water produced in the vicinity of South Pole lake<sup>48</sup> all freezes as it flows downstream and therefore does not contribute to the FIS–AG drainage network. Flow through sediment is not explicitly modelled in GlaDS due to computational limitations, although adjusting the distributed system conductivity can emulate flow through subglacial sediment. There is evidence that some regions of FIS–AG are underlain by marine sediments, but it is suggested that they are not weak and deformable, making GlaDS an applicable model for this region<sup>17</sup>.

We use the ASAID (Antarctic Surface Accumulation and Ice Discharge) grounding line for our domain<sup>42</sup>. The remainder of the domain was determined using hydraulic potential gradients assuming water pressure at overburden and calculating the resulting basal drainage catchments<sup>49</sup> that feed across the grounding lines of IIS, MIS, FIS–AG and SFG. We use outputs from the ISSM, following the methods of Seroussi et al.<sup>15</sup>, which estimate the velocity of ice at the bed (sliding) and refine our triangular mesh in regions where the basal ice flow is greater than  $30 \text{ m yr}^{-1}$  and in the grounding zones of the catchment primary drainage outlets. The minimum mesh edge length is 280 m, and the average for the whole domain is 5.7 km. The basal ice velocity within the catchment ranges from  $0.03 \text{ m yr}^{-1}$  near South Pole to  $627 \text{ m yr}^{-1}$  at the FIS–AG grounding line (Fig. 3a). The basal and surface topography is from BedMachine<sup>14</sup> and encompasses radar data as discussed in ref. <sup>50</sup>,

which gives enhanced bed topography resolution in the FIS–AG region. Other key inputs into GlaDS include the rates of basal water production and basal sliding, the latter driving the rate of distributed system cavity opening/closing. For both of these variables, we use outputs from ISSM model inversions that are spatially variable but temporally constant<sup>15</sup>. The basal water production rate has a maximum of  $0.28 \text{ m yr}^{-1}$  at the FIS–AG grounding line, with large regions of the interior catchment at zero. We assume a temperate bed throughout, which may introduce some errors, but the model does not require active melt production and so areas with zero water production essentially act as frozen regions unless water from up-catchment persists through those elements without refreezing.

There remain many unknowns about basal conditions in the Antarctic, and so we run sensitivity tests to examine the range of likely hydrological conditions in this catchment. Our sensitivity tests include separately varying the conductivity of the distributed system and the channelized system. We also test the role that spatially variable basal water production rates have on the hydrological configuration by running GlaDS with an enhanced water production of 1.5 times the ISSM value. The sensitivity parameter values along with the resulting channel discharge rates at the grounding lines of FIS–AG, IIS, MIS and SFG are shown in Extended Data Table 2. The basal water-pressure and water depth outputs for the sensitivity tests are shown in Fig. 3b–g.

### Radargrams

Airborne radio-echo sounding is a key technique for measuring the morphology and characteristics of beds of large ice sheets. The radar data used in this study were compiled from flight surveys conducted by the CReSIS (Center for Remote Sensing of Ice Sheets) as a part of the NASA Operation IceBridge mission in 2014 and 2016<sup>51</sup>. The MCoRDS (Multichannel Coherent Radar Depth Sounder) was run with a frequency of 195 MHz and a 50 MHz bandwidth<sup>50</sup>. The data were processed assuming homogeneous ice and a radar propagation rate of  $0.168 \text{ m ns}^{-1}$ . Further instrumentation and processing details are provided in ref. <sup>50</sup>. We analyse radio-echo sounding transects across the adjacent ice shelves of IIS, MIS and FIS to chart the geometry of ice-shelf channels across the grounding zone. All elevation measurements (radargram profile and ice surface) are relative to the WGS 84 datum.

### Data availability

BedMachine basal and surface topography DEMs are available at NSIDC. Airborne radar data used in this study are freely available at the CReSIS website (<http://data.cresis.ku.edu/>). Model outputs and reflectivity data are available from the Zenodo repository: <https://doi.org/10.5281/zenodo.6785041>.

### Code availability

The Glacier Drainage System (GlaDS) model code is available by contacting Mauro Werder (werder@vaw.baug.ethz.ch) and is also now included in the Ice-Sheet and Sea-Level System Model (ISSM), which is freely available.

## References

44. Indigo, C., Dow, C. F., Greenbaum, J. S. & Morlighem, M. Drygalski Ice Tongue stability influenced by rift formation and ice morphology. *J. Glaciol.* **67**, 243–252 (2021).
45. Wei, W. et al. Getz Ice Shelf melt enhanced by freshwater discharge from beneath the West Antarctic Ice Sheet. *Cryosphere* **14**, 1399–1408 (2020).
46. Dow, C. F., Werder, M. A., Nowicki, S. & Walker, R. T. Modeling Antarctic subglacial lake filling and drainage cycles. *Cryosphere* **10**, 1381–1393 (2016).
47. Dow, C. F., Karlsson, N. B. & Werder, M. A. Limited impact of subglacial supercooling freeze-on for Greenland ice sheet stratigraphy. *Geophys. Res. Lett.* **45**, 1481–1489 (2018).

48. Siegert, M. J. & Bamber, J. L. Subglacial water at the heads of Antarctic ice-stream tributaries. *J. Glaciol.* **46**, 702–703 (2000).
49. Schwanghart, W. & Kuhn, N. J. TopoToolbox: a set of Matlab functions for topographic analysis. *Environ. Model. Softw.* **25**, 770–781 (2010).
50. Jeofry, H. et al. A new bed elevation model for the Weddell Sea sector of the West Antarctic Ice Sheet. *Earth Syst. Sci. Data* **10**, 711–725 (2018).
51. Radar Depth Sounder Data (CReSIS, 2016); <http://data.cresis.ku.edu/>

## Acknowledgements

We thank M. Werder for use of the Glacier Drainage System (GlaDS) model and M. Morlighem for provision of ISSM basal ice velocity and melt rates. C.F.D. was supported by the Natural Sciences and Engineering Research Council of Canada (NSERC; RGPIN-03761-2017) and the Canada Research Chairs Program (950-231237). M.J.S. and N.R. acknowledge support by the UK Natural Environment Research Council AFI grant NE/G013071/1. N.R. acknowledges funding from the Newcastle University Humanities and Social Science (HASS) bid preparation fund. K.S. was supported by NSERC and the University of Waterloo. We thank Compute Canada for provision of supercomputer resources. We acknowledge the use of data and/or data products from CReSIS generated with support from the University of Kansas, NSF grant ANT-0424589 and NASA Operation IceBridge grant NNX16AH54G.

## Author contributions

C.F.D., N.R., and M.J.S. designed and developed the project and wrote the manuscript. C.F.D. and K.S. ran the model simulations. C.F.D. conducted the analysis and produced the figures. H.J. provided radar data and figures. All authors contributed to editing the manuscript.

## Competing interests

The authors declare no competing interests.

## Additional information

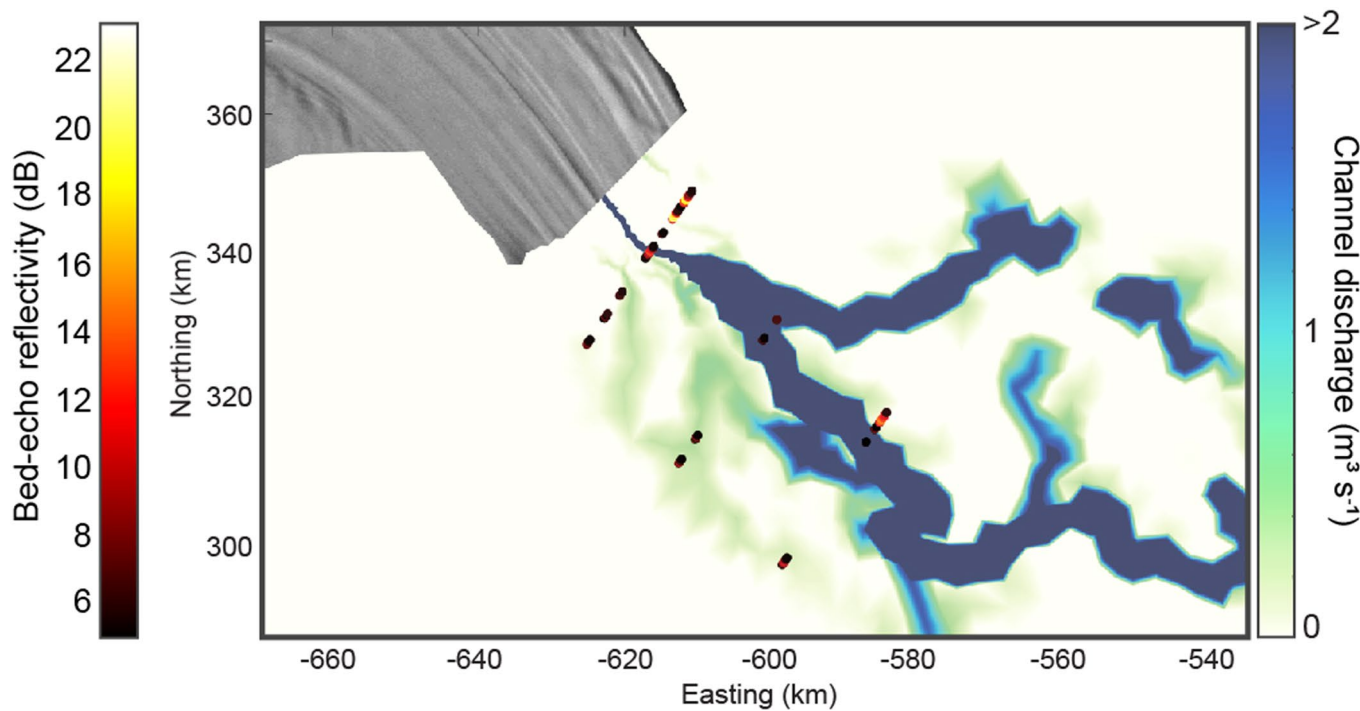
**Extended data** is available for this paper at <https://doi.org/10.1038/s41561-022-01059-1>.

**Supplementary information** The online version contains supplementary material available at <https://doi.org/10.1038/s41561-022-01059-1>.

**Correspondence and requests for materials** should be addressed to C. F. Dow.

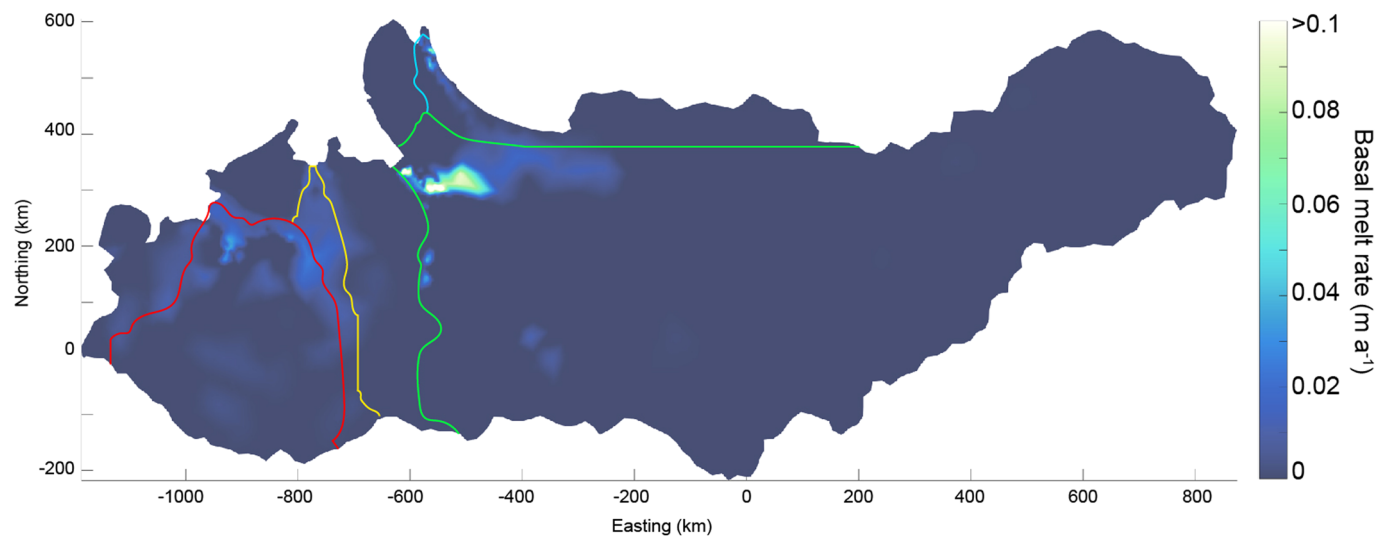
**Peer review information** Nature Geoscience thanks Ian Willis and the other, anonymous, reviewer(s) for their contribution to the peer review of this work. Primary Handling Editor: Tom Richardson, in collaboration with the Nature Geoscience team.

**Reprints and permissions information** is available at [www.nature.com/reprints](http://www.nature.com/reprints).

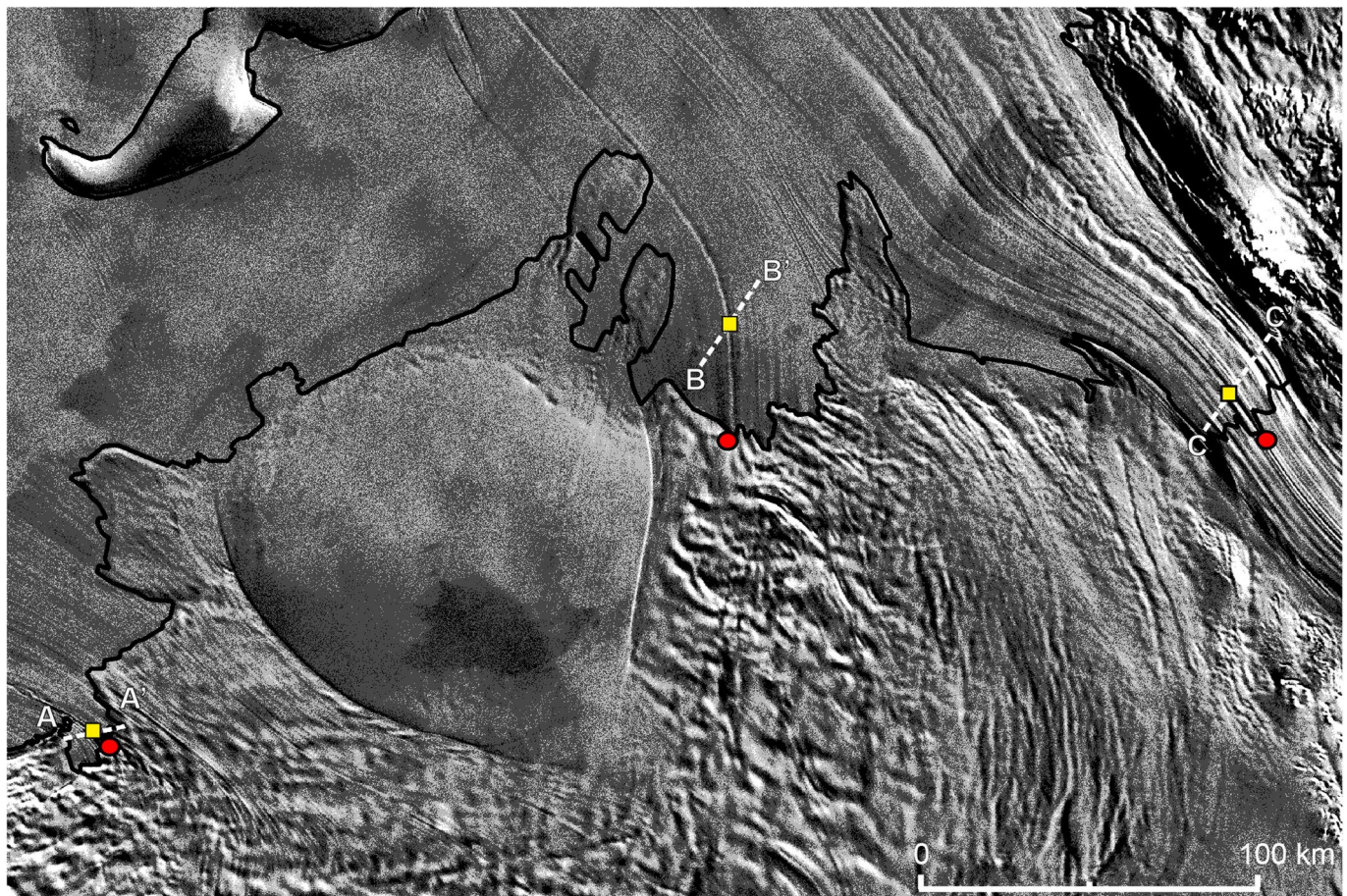
**Extended Data Fig. 1 | Channel discharge compared to radar reflectivity.**

Channel discharge for the FIS-AG catchment for the standard (base) model run. The dots show regions of positive radar reflectivity (calculated as relative values with a zero mean<sup>22</sup>) at the ice-bed interface assumed to indicate the presence of

water<sup>50</sup>; negative relative reflectivity values are not plotted. Background image is the ice surface MODIS mosaic<sup>43</sup>. The extent of this region is shown by the grey box in Fig. 2c.

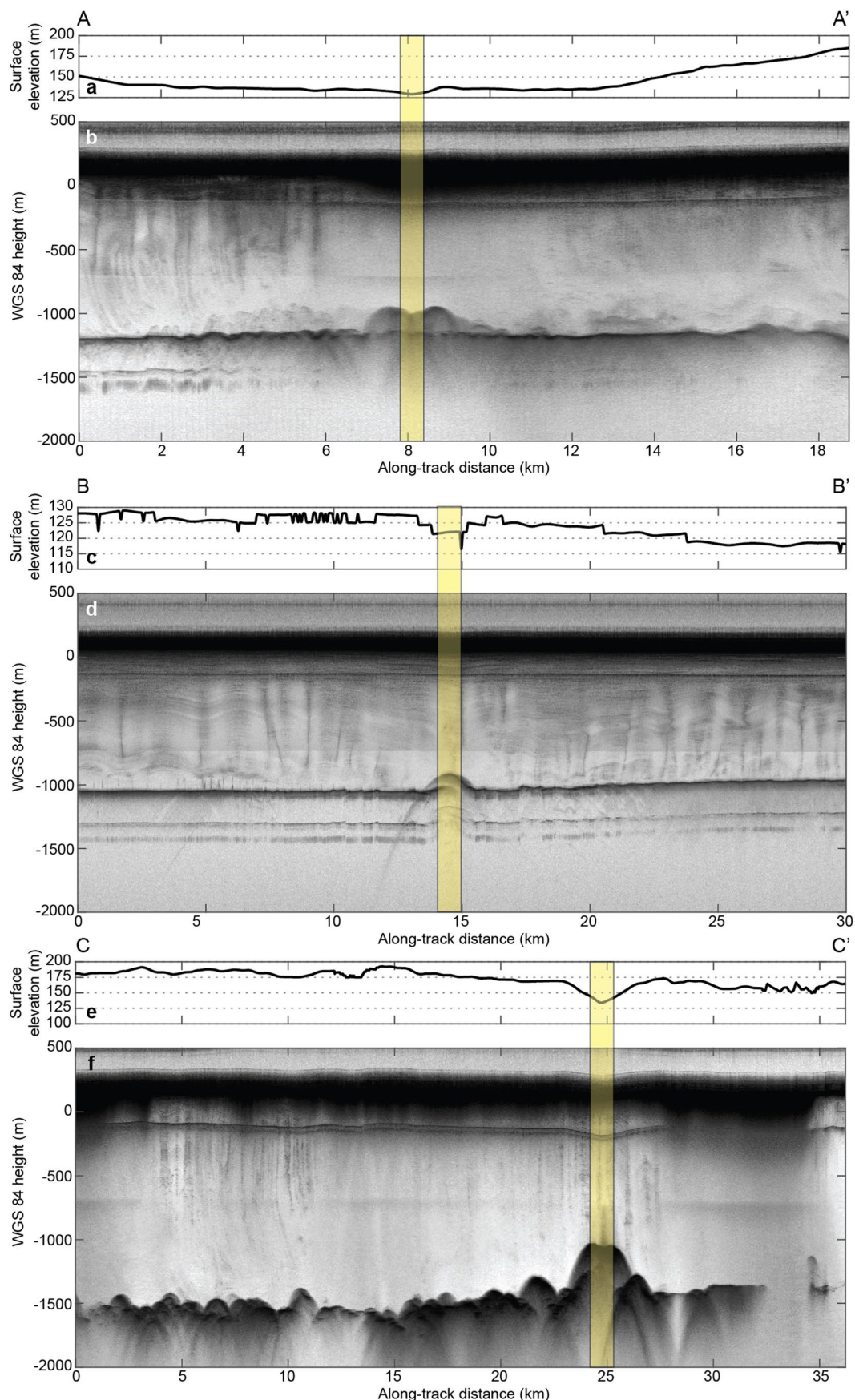


**Extended Data Fig. 2 | Basal melt and hydrology catchments.** Basal melt rate from ISSM<sup>15</sup> with basal drainage catchments outlined for IIS (red), MIS (yellow), FIS-AG (green) and SFG (blue).

**Extended Data Fig. 3 | Location of radar transects shown in Extended Data Fig. 4.**

**Fig. 4.** MODIS ice-surface imagery of the Weddell Sea (WS) sector of West Antarctica<sup>43</sup>. The location of radar transects for IIS (A-A'), MIS (B-B'), and FIS-AG (C-C') are plotted with white dashed lines. These radar transects are shown in

Extended Data Fig. 4. The red dots are the location of modelled channel outlets over the grounding line (Fig. 2c, d) and the yellow squares, the location of sub ice-shelf channels (shown as yellow bars in Extended Data Fig. 4).


**Extended Data Fig. 4 | Ice shelf radar transects with incised basal channels.**

Channels are incised upwards beneath floating ice for the following ice streams: (a,b) IIS (A-A'), (c,d) MIS (B-B'), and (e,f) FIS-AG (C-C'), with transects shown in Extended Data Fig. 3. Surface elevation profiles from an aircraft altimeter are

plotted above each radargram (a,c,e) with depressions as a result of hydrostatic adjustment from the incised basal channels. Yellow bars show the location of the ice shelf channel as indicated by the yellow boxes in Extended Data Fig. 3.

**Extended Data Table 1 | GlaDS model parameters (base model run)**

Parameter	Value	Units
Bedrock bump height	0.08	m
Cavity spacing	2	m
Channel conductivity	$5 \times 10^{-2}$	$\text{m}^{3/2} \text{ kg}^{-1/2}$
Englacial void ratio	$10^{-5}$	
Glen's flow constant	3	
Ice density	910	$\text{kg m}^{-3}$
Ice flow constant	$2.5 \times 10^{-25}$	$\text{Pa}^3 \text{ s}^{-1}$
Sheet conductivity	$1 \times 10^{-4}$	$\text{m}^{7/4} \text{ kg}^{-1/2}$
Sheet width below channel	2	m

Extended Data Table 2 | Grounding line discharge rates for model sensitivity tests

Parameter	Value	Units	FIS-AG ( $\text{m}^3 \text{s}^{-1}$ )	IIS ( $\text{m}^3 \text{s}^{-1}$ )	MIS ( $\text{m}^3 \text{s}^{-1}$ )	SFG ( $\text{m}^3 \text{s}^{-1}$ )
Base model			24.18	8.28	3.90	0.51/0.45
Sheet conductivity	$8 \times 10^{-5}$	$\text{m}^{3/2} \text{ kg}^{-1/2}$	23.54	9.12	4.15	0.41/0.38
(lower)						
Channel conductivity	$1 \times 10^{-1}$	$\text{m}^{3/2} \text{ kg}^{-1/2}$	22.33	8.32	3.74	0.49/0.46
(high)						
Channel conductivity	$1 \times 10^{-2}$	$\text{m}^{3/2} \text{ kg}^{-1/2}$	11.65	8.32	4.96	0.43/0.18
(low)						
Increased water input	Base *1.5	$\text{m}^3 \text{ yr}^{-1}$	32.30	15.50	5.87	0.83/0.59

## Extended Data Table 3 | Catchment and grounding zone calculations

	<b>FIS-AG</b>	<b>IIS</b>	<b>MIS</b>	<b>SFG</b>
Catchment area (km <sup>2</sup> )	614,000	125,000	20,000	52,000
Water production rate (m <sup>3</sup> s <sup>-1</sup> )	18.7	10.1	4.80	2.3
Channel discharge volume (m <sup>3</sup> s <sup>-1</sup> )	24.18	8.28	3.90	0.51/0.45
Ice shelf channel height (m)	400	210	160	170
Distance of measured ice shelf channel from grounding zone (km)	10	0	35	7
Cryosat-2 channel outlet ice shelf melt rate <sup>36</sup> (m yr <sup>-1</sup> )	26.43	1.9*	1.1	18.5/16.4
Ocean model <sup>37</sup> grounding zone melt rate (m yr <sup>-1</sup> )	2.9	0.4	0.4	2.8

\*value 3 km from grounding line due to lack of Cryosat-2 data